

Image correlation by one-dimensional signatures invariant to rotation, position, and scale using the radial Hilbert transform optimized

ALFREDO CASTRO-VALDEZ,¹ JOSUÉ ÁLVAREZ-BORREGO,^{1,*} AND SELENE SOLORZA-CALDERÓN²

¹Applied Physics Division, Optics Department, CICESE, Carretera Ensenada-Tijuana No. 3918, Fraccionamiento Zona Playitas, Ensenada C. P. 22860, Mexico

²Facultad de Ciencias, Matemáticas Aplicadas, UABC, Ensenada, Mexico

*Corresponding author: josue@cicese.mx

Received 25 October 2019; revised 10 December 2019; accepted 16 December 2019; posted 16 December 2019 (Doc. ID 381574); published 24 January 2020

This paper presents a new methodology for pattern recognition invariant to rotation, position, and scale. The method uses the correlation of signatures, where the signatures were created with a new equation called the radial Hilbert transform optimized (RHTO) for longer signatures. An analysis with eight non-homogeneous illumination patterns was performed with 2000 letter variants and 30 phytoplankton species. The higher confidence level was founded using the radial Hilbert optimized methodology. Also, it utilized a correlation called adaptive linear–nonlinear correlation, which gave a better discrimination performance than the nonlinear correlation function. © 2020 Optical Society of America

<https://doi.org/10.1364/AO.381574>

1. INTRODUCTION

People can identify objects and classify them in different ways. In this manner, the information can be better managed. However, the images rarely share the same scale or rotation. It is easy for us to ignore these differences. Still, a computer system cannot do it so quickly. The study of complex images and patterns has multiple applications in the area of optics.

Several methods have been developed in search of invariances of scale, shift, and rotation [1–4]. Mathematical transformations are required to produce these invariances. The modulus of the Fourier transform [5] and the modulus of the Mellin transform yield invariance to displacement and scale, respectively [6,7]. Rotational invariance can be achieved with some binary ring masks [8–11].

Each methodology can have several invariances. However, the confidence level in each method can vary. The images to identify can have some previous treatment to increase the confidence level in the identification. The Hilbert transform highlights the edges and borders; this can help with the identification of objects [12,13], and the Hilbert radial transform has been used to detect the corners of images when they present rotations [14–16].

Another factor in the recognition of images is the correlation filters. From the classic filter [17], to the phase-only filter [18], to the multiple filters that now exist, the applications are varied since each one has a different quality.

The computation time is an essential factor too. Since the images used have better quality, which implies more data to evaluate, the computation time could render a methodology non-viable. The signatures used reduce that time and are still capable of recognizing images. In this work, a system is proposed to distinguish between images using signatures, which produces a more efficient recognition capability.

The material of this work is organized as follows: in Section 2, the state of the art is described, and Section 3 describes the methodology; in Sections 3A and 3B, the creation of signatures using RHTO is written, and the adaptive linear–nonlinear correlation is explained; in Sections 4 and 4A, the results and discussion are presented, and a comparison analysis is done; in Section 5, the conclusions are given.

2. STATE OF THE ART

Binary masks were used to obtain rotation or scale invariances [19]; these masks were applied in pulmonary diseases [20]. A combination of these masks was proposed by the authors of Ref. [21], who used two binary masks: one with concentric rings and another with circumference transects. This combination was named a ring wedge detector (RWD), which consists of two half-circle regions; one semicircle is composed of a series of concentric rings, and the other was formed with circumferential transects separated by equidistant angles.

The RWD mask is invariant to rotation and scale, but when the images have distortions of scale and rotation combined, the results are complicated to interpret.

Scale invariance is achieved using log-polar mapping as a pre-processing process followed by a Fourier transform [22–24]. In Ref. [25], the authors were the first to use the discrete Fourier transform followed by a log-polar mapping of an input image to approximate the Mellin transform.

Mellin’s transform proposal was given by the authors of the Ref. [26], who combined it with the Fourier transform to obtain invariances to scale and position. Then the scale transform was developed by the author of Ref. [27], who found this as a particular case of the Mellin transform.

This methodology was used to identify objects using a phase correlation by the scale transform spectrum to automatic character recognition [28]. This methodology produces scale, rotation, and position invariances.

Different applications of digital the Mellin transform and scale transform were published [29–31]. The authors of Ref. [32] described the Mellin and scale fast transform, which reduces the computational time by the implementation of the Fourier transform in their algorithm.

In 2009 two authors developed vector signatures based on the properties of Fourier and scale transform [33] for the recognition of patterns invariant to position, rotation, and scale. In Ref. [34], the authors compared different types of letters using nonlinear correlation with rotation and scale invariances.

In 2014, the authors of Ref. [35] developed and implemented a new correlation type named adaptive nonlinear correlation to classify signatures created by binary masks using the scale transform. This methodology was tested with phytoplankton species and produced a better performance than a nonlinear correlation. In 2014, using the polar Mellin transform, the authors of Ref. [36] detected objects with different scale and rotation, and in 2019, the authors of Ref. [37] demonstrated that, using a hybrid optoelectronic correlator, objects with variances in shift, size, and rotation can be recognized.

In Ref. [38], the authors used a Fourier–Mellin transform and radial Hilbert transform and tested them using a butterfly database. Binary masks were created using the fractional Fourier transform [39].

3. METHODOLOGY

A problem in pattern recognition is that the computer cannot identify an object when it has distortions; computers detect the same objective as a different one. We used a methodology to determine if it is possible to not only recognize images with rotations, scales, and displacements but also to have better results to classify them. This methodology uses different transforms to obtain the required invariances. The Mellin transform has scale invariance; the Fourier transform has displacement invariance, and the radial Hilbert transform has rotation invariance; with this, the input image is turned into a signature. The signatures have very few values in comparison with images. If a signature can represent an image with a high capability of recognition, the time it takes to compare them will be lower than using images.

Using various integral transforms for images, correlations with different invariances could be achieved. One possibility

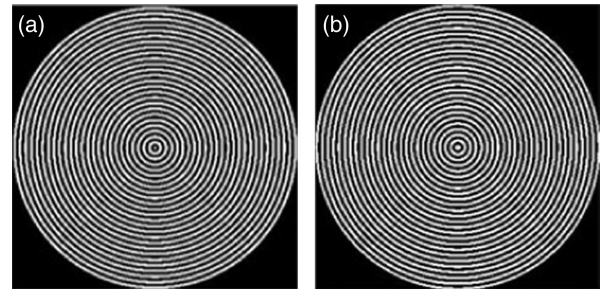


Fig. 1. Concentric rings of the radial Hilbert transform with $\Phi(\theta, r) = e^{ir\theta}$: (a) from the real part; (b) from the imaginary part.

is to use the modulus of the Fourier transform, as it has the property of shift-invariance.

The Mellin transform is defined as [7]

$$\mathbb{M}[f(k, v)] = \frac{1}{2\pi} \int_0^\infty \int_0^{2\pi} f(r, \theta) r^{-iv} e^{-ik\theta} d\theta \frac{dr}{r}. \quad (1)$$

One of the most important properties of this transformation is that the scale changes become a phase.

The 2D Radial Hilbert transform (\mathbb{H}_R) is presented as [15]

$$\mathbb{H}_R[g(x_1, x_2)] = \mathbb{F}^{-1}[H(\omega, s) G(\omega, s)], \quad (2)$$

where $H(\omega, s) = \Phi(\theta, r)$ is an arbitrary radial function and $G(\omega, s)$ is the Fourier transform of $g(x_1, x_2)$. (x_1, x_2) and (ω, s) represent spatial and frequency coordinates, respectively. In the particular case where $\Phi(\theta, r) = e^{ir\theta}$, we obtain, according to the authors of [22],

$$g_H(x_1, x_2) = \mathbb{H}_R[g(x_1, x_2)] = \mathbb{F}^{-1}[e^{ir\theta} G(\omega, s)], \quad (3)$$

where $\theta = \arccos(\frac{\omega}{r})$, $r = \sqrt{\omega^2 + s^2}$ to each $(\omega, s) \neq (0, 0)$, and $\theta = 0$ in $H(0, 0)$.

Equation (2) produces a complex function $H(\omega, s)$, which can be represented as

$$\Phi(\theta, r) = H(\omega, s) = \text{Re}[H] + i\text{Im}[H]. \quad (4)$$

Multiplying these values by a unitary disc with dimension r produces two masks (real and imaginary parts) of concentric rings defined by the dimension of $f(x_1, x_2)$ (Fig. 1).

The radial Hilbert transform optimized (RHTO) is presented in this paper with a parameter α , which changes the rings number, as follows:

$$\Phi(\theta, r) = e^{ir^\alpha\theta}. \quad (5)$$

The α value has an optimal range; to find that range, different values of α were tested, and we graphed their binary mask results (Fig. 2).

The number of rings is related to the signature length and the autocorrelation value of the signature. Figure 3 shows the signature using the binary masks in Fig. 2. However, more rings could be analyzed, but we can find some errors (Fig. 3f) where the signature is no longer. Two graphs were created to find the optimal value of α in which the ring number is maximum; this value is related to the signature length. Also, the maximum auto-correlation value was evaluated, and both parameters were calculated for the real part mask (Figs. 4 and 5), obtaining

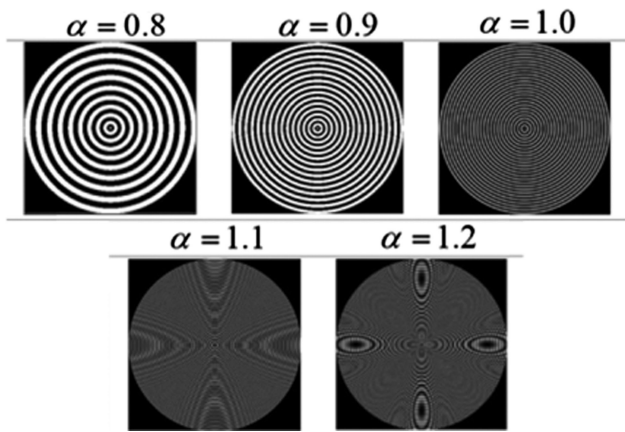


Fig. 2. Real part masks with different numbers of rings obtained by different values of α .

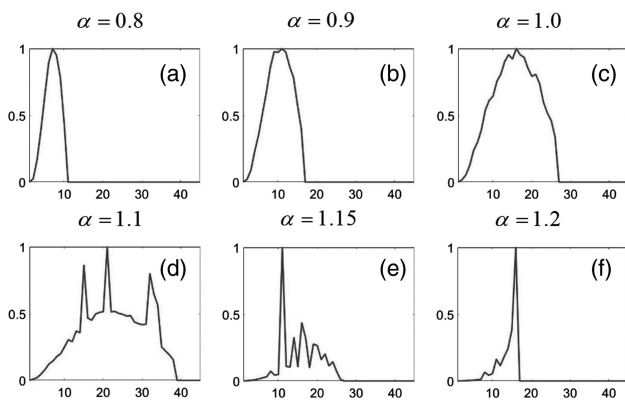


Fig. 3. Signatures from the real part mask S_{HR} of the same image obtained by different values of α .

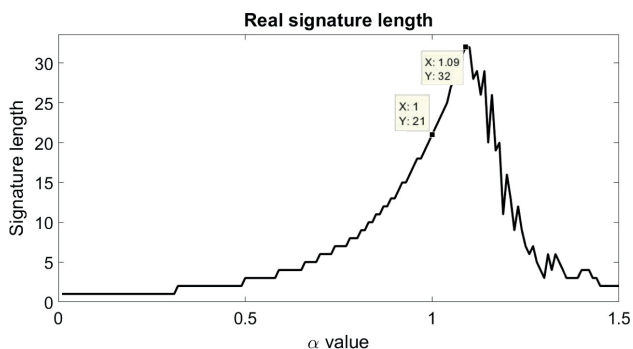


Fig. 4. Lengths of signatures S_{HR} with different values of α from 0.01 to 1.5.

the value $\alpha = 1.09$ for both cases. This value is the same for all different geometries.

A. Creation of Signatures Using RHTO

The signatures were created using the Fourier transforms, the Mellin transforms, and RHTO (see Fig. 6). First, the size of the input image (A) was taken using the RHTO

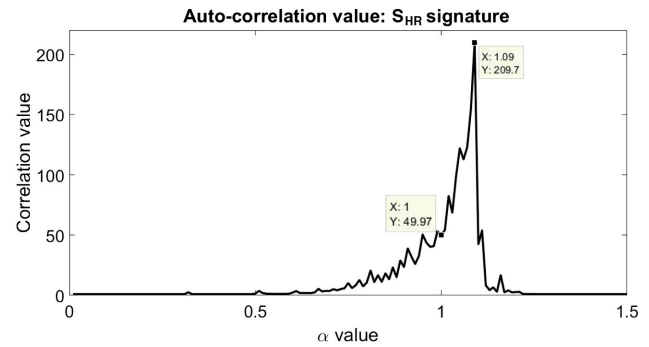


Fig. 5. Auto-correlation values of signatures S_{HR} with different values of α from 0.01 to 1.5.

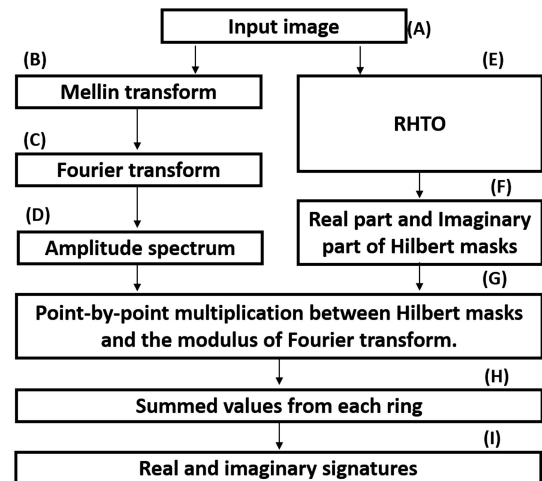


Fig. 6. Scheme to create an optimized signature of an input image.

part and the imaginary part of binary rings masks (F). Then, the Mellin transform (B), followed by the Fourier transform (C), was applied to the input image. The modulus of this result (D) was taken and was multiplied point by point with the binary rings mask (G). Finally, for the two masks, the values in each ring were summed (H) to obtain the signature of the input image and obtain signature by mask, which were called: real signature S_{HR} and imaginary signature S_{HI} (I). These signatures are invariant to rotation, scale, and position.

Using an S_{HR} signature, the optimal α value found was 1.09 for signature length and auto-correlation value.

Different letters in Arial font with 10 scales and 40 rotations were transformed into signatures to probe this methodology. To examine the methodology response using images with non-homogeneous illumination, eight illumination patterns, which simulate the typical light variations, were tested (see Fig. 7). The signatures of the letter E with some rotations and scales are shown in Fig. 8a, and Fig. 8b shows variations of the signature with illumination.

The letters B, E, F, H, and P were used with 400 variations. Each letter had differences in scale from 75% to 130% and 40 rotations between 0° and 355° . Figure 9 shows some variations of the letter B. Two thousand signatures were created with

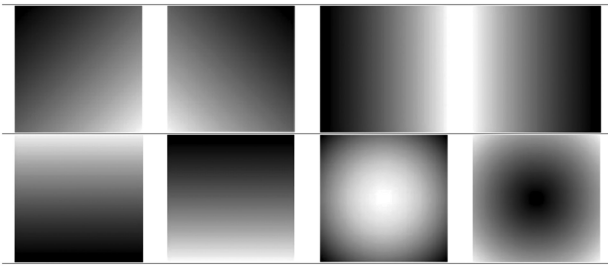


Fig. 7. Non-homogeneous illumination patterns used with rotated and scaled images.

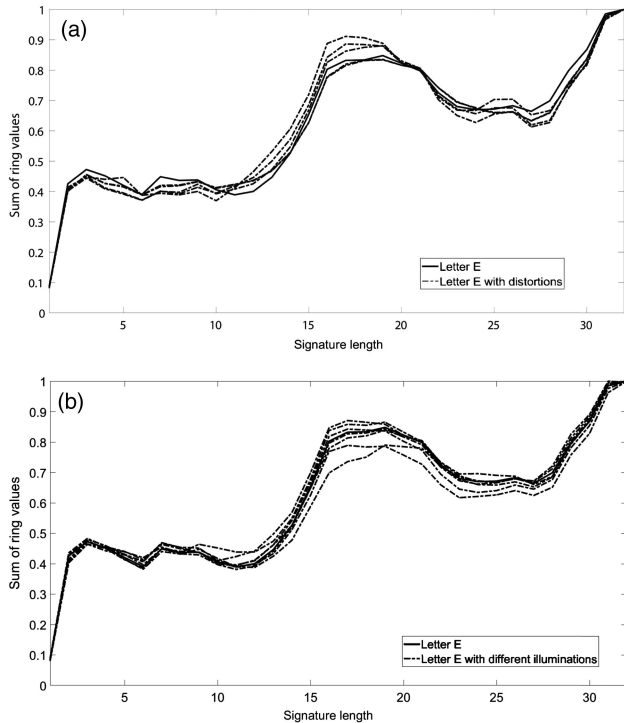


Fig. 8. Signatures S_{HR} from the letter E: (a) with different scales and rotations; (b) with different illumination.

RHTO and with the conventional radial Hilbert transform ($\alpha = 1$) to be used in the classification step.

The 2000 letter images were multiplied by the illumination patterns showed in Fig. 7 to create 18,000 images, which were transformed into 18,000 signatures to correlate (eight illumination patterns + the original image) to compare the capability of detection for letters immersed in different illumination. The illumination patterns chosen to be examined were from other results given by authors in [40] and [41] to were chosen to simulate different non-homogeneous illuminations found in pictures.

A second image group was created using 30 phytoplankton species with 576 variations in each species (Fig. 10). Phytoplankton is of great ecological significance since it constitutes the greatest portion of primary producers in the sea.

Each image was rotated 360° with 5° steps and scaled 8 times from 80% to 115% in 5% steps. Every picture was transformed into a signature.

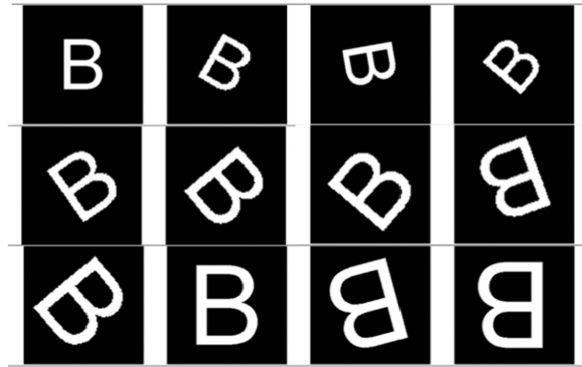


Fig. 9. Different variations of the letter B used to create signatures.

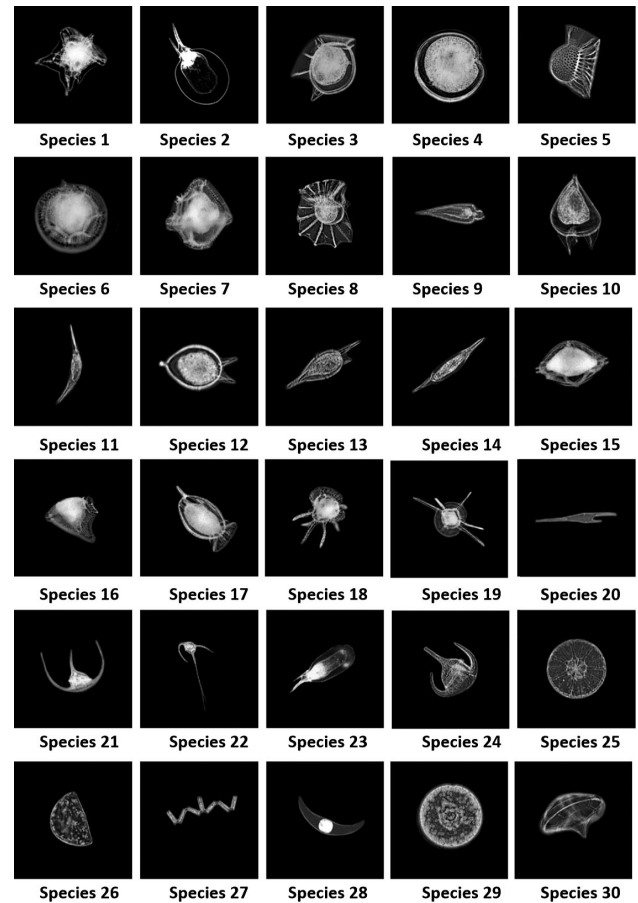


Fig. 10. Phytoplankton species used in correlation. The names of the phytoplankton names are listed in Table 1.

A third image group was considered using 20 random species of natural phytoplankton with variations in scale from 90% to 110% in 5% steps and rotations of 0° – 355° in 5° steps (Fig. 11). These images have natural noise and natural illumination.

B. Adaptive Linear–Nonlinear Correlation

A linear–nonlinear correlation was proposed in this work to produce superior performance in comparison with the classical filter techniques regarding discrimination capability. In Fig. 12,

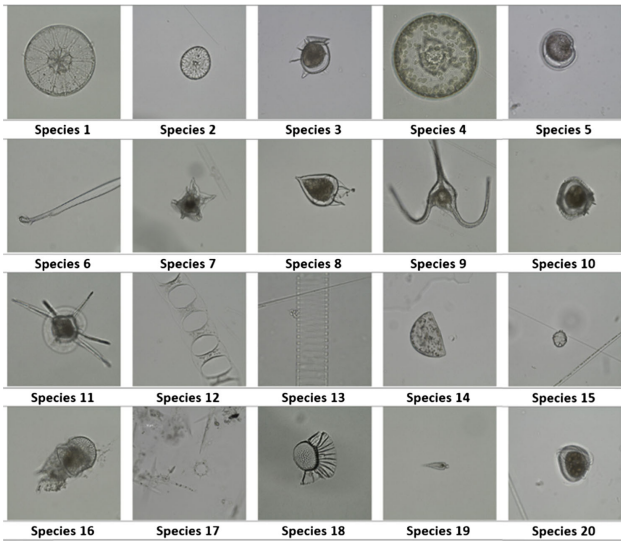


Fig. 11. Phytoplankton species from a third group used in correlation. The names of the phytoplankton are listed in Table 2.

Table 2. Species Names from the Third Phytoplankton Group

Species 1	Asterolampra marylandica	Species 11	Ceratocorys horrida
Species 2	Asteromphalus heptactis	Species 12	Climacodium
Species 3	Dinophysis hastata	Species 13	Dactyliosolen antarcticus
Species 4	Hemidiscus	Species 14	Hemidiscus cuneiformis
Species 5	Diplosalopsis lenticulatum	Species 15	Goniaulax scrippsae
Species 6	Amphisolenia bidentate	Species 16	Heterodinium
Species 7	Acanthogonyaul spinifera	Species 17	Octaris octonaria
Species 8	Podolampas bipes	Species 18	Ornithocercus steinii
Species 9	Ceratium macroceros	Species 19	Oxytoxum scolapax
Species 10	Ceratocorys hastata	Species 20	Phalacroma cuneus

Table 1. Species Names from the Phytoplankton Group

Species 1	Acanthogonyaulax spinifera	Species 16	Dinophysis rapa
Species 2	Ceratium gravidum	Species 17	Dinophysis hastate
Species 3	Dinophysis hastata	Species 18	Ceratocorys horrida
Species 4	Diplosalopsis orbicularis	Species 19	Ceratocorys horrida 2
Species 5	Histioneis	Species 20	Ceratium furca
Species 6	Lingolodinium polyedrum	Species 21	Ceratium lunula
Species 7	Ornithocercu armata	Species 22	Ceratium hexacatum
Species 8	Ornithocercus magnificus	Species 23	Ceratium praelongum
Species 9	Oxytoxum scolapax	Species 24	Ceratium breve
Species 10	Podolampas bipes 1	Species 25	Asterolampra marylandica
Species 11	Podolampas Spinifer	Species 26	Hemidiscus cuneiformis
Species 12	Podolampas bipes 2	Species 27	Thalassionema nitzschoides
Species 13	Podolampas palmipes	Species 28	Pyrocystis
Species 14	Podolampa spinifer	Species 29	Hemidiscus
Species 15	Protoperidinium	Species 30	Dinoflagellata

first, with the target signature (A), its standard deviation is calculated (B). The same is also done for the problem signature (C), (D). With both standard deviations, the Rz factor is calculated (E); this factor is compared with the Index_σ (F), and, if the Rz factor is greater than or equal to Index_σ , then the factor changes to 1 and otherwise retains its value. Then the Fourier transform is applied to the target signature (G), and its complex conjugate

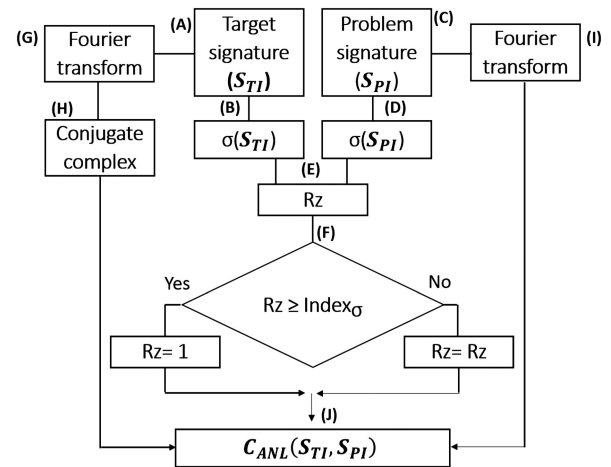


Fig. 12. Procedure to correlate the phytoplankton signatures using an adaptive linear–nonlinear correlation system.

is calculated (H). The Fourier transform is applied to the problem signature (I), and an adaptive linear–nonlinear correlation is made (J); if the Rz factor is 1, it is a linear correlation, and it is nonlinear for values of Rz different from 1. To recognize the target, the signature of the problem image (S_{PI}) is compared with the signature of the target image (S_{TI}) using the adaptive linear–nonlinear correlation (C_{ANL}), that is,

$$C_{ANL} = \mathbb{F}^{-1} \left\{ |F(S_{PI})|^{Rz} \exp(i\phi_{S_{PI}}) \times |F(S_{TI})| \exp(-i\phi_{S_{TI}}) \right\}, \quad (6)$$

where

$$Rz = \begin{cases} \frac{\sigma_{PI}}{\sigma_{TI}}, & \sigma_{PI} \leq \sigma_{TI} \\ \frac{\sigma_{TI}}{\sigma_{PI}}, & \sigma_{PI} > \sigma_{TI} \end{cases}, \quad (7)$$

where σ_{PI} , σ_{TI} are the standard deviations of S_{PI} , S_{TI} and $\phi_{S_{PI}}$, $\phi_{S_{TI}}$ are the phases of S_{PI} , S_{TI} .

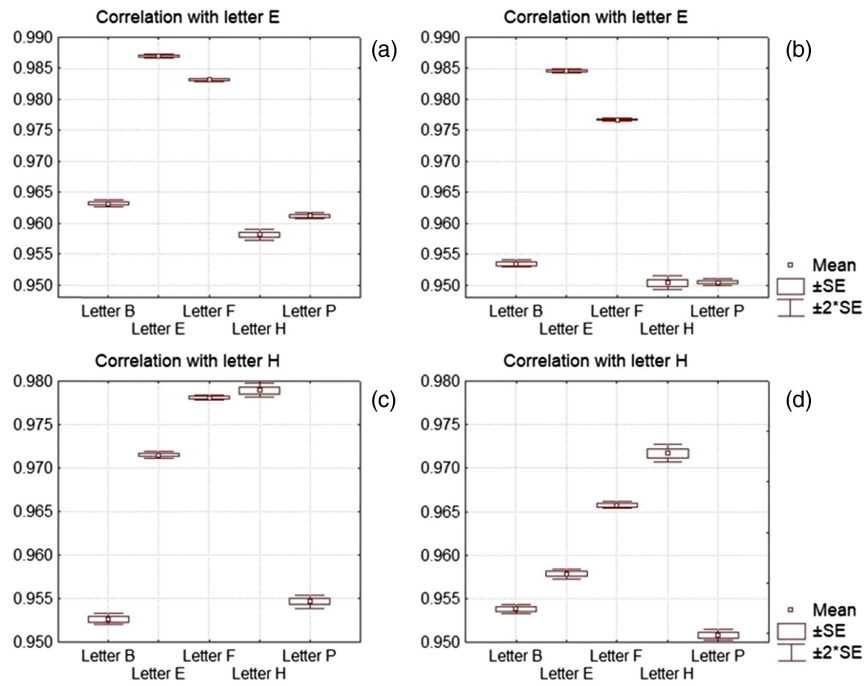


Fig. 13. Correlation average values: (a), (c) using the conventional radial Hilbert transform and (b), (d) with the radial Hilbert transform optimized.

The Rz factor is proposed as a selector for correlating the signatures. If the Rz value was in a range to a determinate species used as a filter, this factor was changed to 1, and the correlation signatures were applied with a linear correlation. If the value of Rz was out of the range, this value was conserved, and this produced a nonlinear correlation in which the discrimination values decreased and increased the correlation performance. The range to change Rz depended on an index of the different standard deviations of the signatures. The index is given by

$$\text{Index}_\sigma = \min(S_{T1}^*), \tag{8}$$

where Index_σ is the minimum correlation values of all variations of the standard deviation of the target signature and S_{T1}^* represents those variations.

4. RESULTS AND DISCUSSION

Each letter signature taken as the target fitted a reference scale of 100% and rotation of zero degrees.

Each one was compared to the 18,000 letter signatures through two methods ($\alpha = 1$ and α optimized). It was found that it is better to work with the RHTO method ($\alpha =$ optimized). The RHTO method gives a confidence level higher than that of the conventional radial Hilbert transform (Fig. 13). For example, the letter H cannot be identified correctly (Fig. 13c). Other letters had a lower confidence level than the optimized methodology.

Figure 13 shows that the conventional Hilbert transform had a disadvantage versus the RHTO methodology because the length of the signatures created with the conventional method

is shorter than that of the RTHO; thus, it has less information. In Fig. 13b, the correlation values between letters are lower than in Fig. 13a, creating a better discrimination level. The adaptive linear–nonlinear correlation was used with the phytoplankton group. Species with scale 100% and rotation 0° were used as target signatures. For calculating the Index_σ , the standard deviation of each variation of the same species was calculated with Eq. (8).

For each correlation, the value was transformed by the Z-Fisher transform [42] with a 99.9% confidence level. For each species, the maximum and minimum ρ values using every variation were graphed. Because the correlation values are contained in a box with 99.9% of their dispersion within, if the graph does not have an overlap, the confidence level is more than 99.9%. In the filter species, the maximum ρ value and the mean of the minimum value were graphed. The purpose of taking the mean of the minimum correlation values is to compensate for the lower values obtained by the poorly taken images. Using this consideration, we can select better images to compare between species. Applying these considerations, a 99.9% confidence level was found for the 30 species.

The boxes in Fig. 14 show the maximum and minimum ρ values with a 99.9% dispersion contained within; this is a 99.9% confidence level. In every case, the target signature could be recognized. The highest values of ρ can be observed for the filter species, which is marked with the black arrow in both cases. The results are similar to the 30 species correlated with RHTO signatures, adaptive linear–nonlinear. No correlated species showed overlaps between them.

The same results were obtained for natural image analysis (Fig. 15).

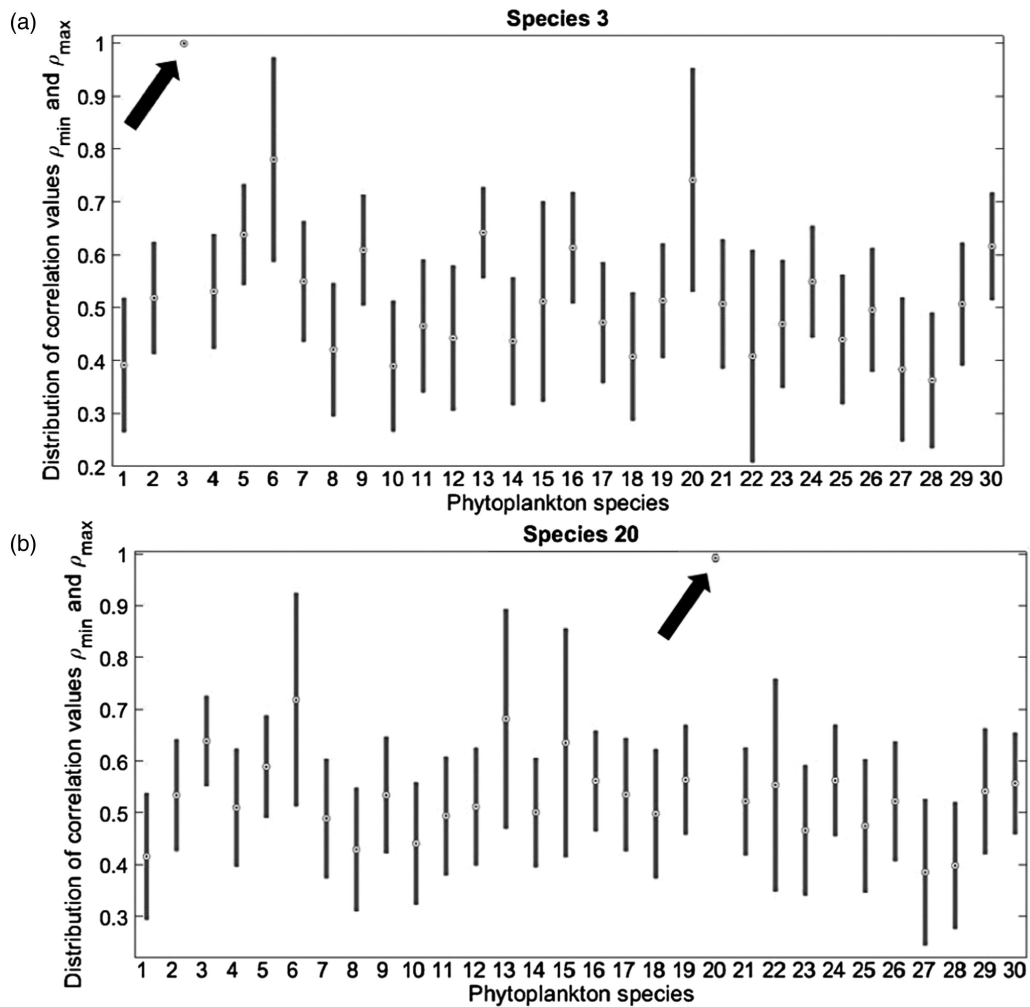


Fig. 14. ρ values between different phytoplankton images using the Z-Fisher transform and adaptive nonlinear filter: (a) using species 3 as the target; (b) using species 20 as the target.

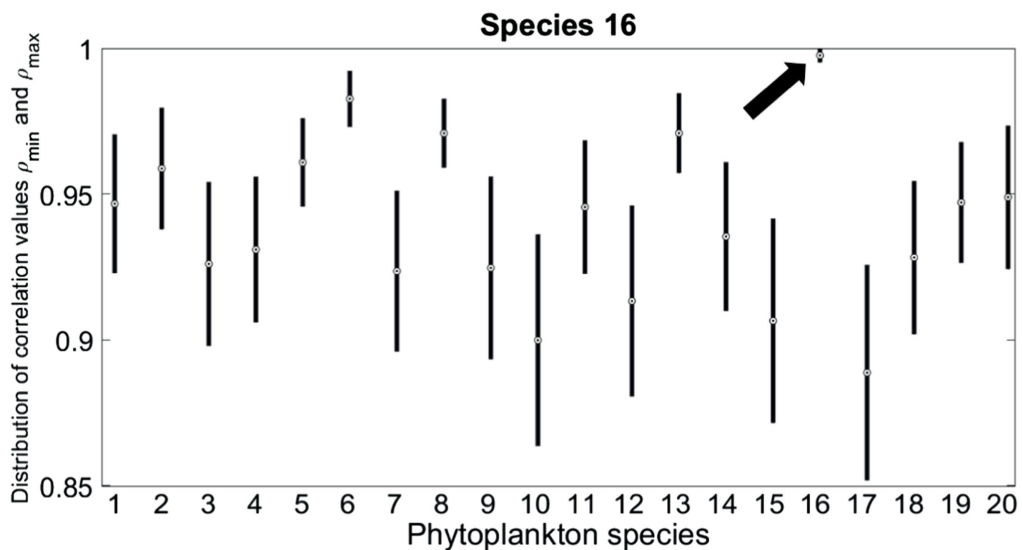


Fig. 15. ρ values between different natural phytoplankton images using the Z-Fisher transform and adaptive nonlinear filter using species 16 as the target.

A. Comparison Analysis

The time consumption was 86 ms for the conventional signatures and 90 ms for the RHTO signatures; using a 320 pixel \times 320 pixel input image, the signature correlation is faster than image correlation, and the mean time consumption per correlation was 58 μ s using this methodology. The times were obtained on a Windows 10 computer with a 3.4 GHz Intel i7-3770 with 8GB RAM. These methods are invariant to position, rotation, and scale. Comparing the methods with those proposed by [35], our accuracy is above 99.9%, 3 standard deviations using the Z-Fisher transform and the adaptive linear–nonlinear correlation, versus the 95.4% obtained by [35] and [38].

5. CONCLUSIONS

The results show that modifying the radial Hilbert transform can optimize the number of rings and produce a more characteristic signature that discriminates against other representative signatures with a high confidence level. In this work, the optimal value of α was 1.09 to provide a more extended signature. This value is the same in auto-correlation value and maximum length signature metrics.

Longer signatures had more information to correlate; this produces a better confidence level than the signatures created with the conventional radial Hilbert transform. The time to calculate the RHTO is the same in comparison with the conventional radial Hilbert transform. The images used were letters and phytoplankton pictures with different scales and rotations. With the letters, the RHTO methodology was capable of recognizing them with an average confidence level of up to 95%. With the phytoplankton images, the correlation values were evaluated with the Z-Fisher transform, and we found a confidence level up to 99.9% in the 30 species. This methodology can be used to obtain more information from an image transformed into a signature. This method and adaptive linear–nonlinear correlation produce excellent discrimination capability for the target signature.

Funding. Centro de Investigación Científica y de Educación Superior de Ensenada, B. C. (CICESE).

Acknowledgment. This study has been included in the thesis supported by CONACyT under the scholarship 591816. Alfredo Castro-Valdez is a student of the Ph.D. program of the Optics Department in CICESE and CONACyT's scholarship with CVU: 690311.

Disclosures. The authors declare no conflicts of interest.

REFERENCES

- R. E. Guerrero-Moreno and J. Álvarez-Borrego, "Nonlinear composite filter performance," *Opt. Eng.* **48**, 067201 (2009).
- C. Fimbres-Castro, J. Álvarez-Borrego, and M. A. Bueno-Ibarra, "Invariant nonlinear correlation and spectral index for diatoms recognition," *Opt. Eng.* **51**, 047201 (2012).
- C. Fimbres-Castro, J. Álvarez-Borrego, I. Vazquez-Martinez, T. L. Espinoza-Carreón, A. E. Ulloa-Pérez, and M. A. Bueno-Ibarra, "Nonlinear correlation by using invariant identity vectors signatures to identify plankton," *Gayana* **77**, 105–124 (2013).
- B. Yang, T. Suk, J. Flusser, Z. Shia, and X. Chen, "Rotation invariants from Gaussian–Hermite moments of color images," *Signal Processing* **143**, 282–291 (2017).
- R. Bracewell, *Fourier Analysis and Imaging*, 3rd ed. (Springer, 2000).
- J. J. K. O'Ruanaidh and T. Pun, "Rotation, scale and translation invariant digital image watermarking," in *Proceedings of International Conference on Image Processing*, 1997, Vol. 1, pp. 536–539.
- S. Derrode and F. Ghorbel, "Robust and efficient Fourier–Mellin transform approximations for gray-level image reconstruction and complete invariant description," *Comp. Vision and Image Understanding* **83**, 57–78 (2001).
- S. Solorza and J. Álvarez-Borrego, "Digital system of invariant correlation to position and rotation," *Opt. Commun.* **283**, 3613–3630 (2010).
- S. Solorza, J. Álvarez-Borrego, and G. Chaparro-Magallanez, "Pattern recognition of digital images by one-dimensional signatures," in *Fourier Transform-Signal Processing*, San Luis Potosí, Mexico, September 19–21, 2012, Chap. 13.
- J. Álvarez-Borrego, S. Solorza, and M. A. Bueno-Ibarra, "Invariant correlation to position and rotation using a binary mask applied to binary and gray images," *Opt. Commun.* **294**, 105–117 (2013).
- S. Solorza and J. Álvarez-Borrego, "Position and rotation-invariant pattern recognition system by binary rings masks," *J. Modern Opt.* **62**, 851–864 (2015).
- C.-C. Tseng and S.-C. Pei, "Design and application of discrete-time fractional Hilbert transformer," *IEEE Trans. Circuits Syst. II, Analog Digit. Signal Process.* **47**, 1529–1533 (2000).
- A. Montes Pérez, G. Rodríguez Zurita y, and A. Martínez García, "Reconstrucción tomográfica con realce de bordes isotrópicos de objetos de fase mediante la transformada de Hilbert," in *IV Congreso Nacional de Tecnología Aplicada a Ciencias de la Salud, Tonantzintla, Cholula, Puebla, Mexico*, 2013.
- K. Kohlmann, "Corner detection in natural images based on the 2-D Hilbert transform," *Signal Processing* **48**, 225–234 (1996).
- J. A. Davis, D. E. McNamara, and D. M. Cottrell, "Image processing with the radial Hilbert transform: theory and experiments," *Opt. Lett.* **25**, 99–101 (2000).
- S.-C. Pei and C.-C. Tseng, "The generalized radial Hilbert transform and its applications to 2D edge detection (any direction or specified directions)," in *IEEE International Conference on Acoustics, Speech, and Signal Processing*, 2003, Vol. 3, pp. III-357.
- A. Vander Lugt, "Signal detection by complex spatial filtering," *IEEE Trans. Inf. Theory* **10**, 139–145 (1964).
- J. L. Horner and P. D. Gianino, "Phase-only matched filtering," *Appl. Opt.* **23**, 812–816 (1984).
- G. G. Lendaris and G. L. Stanley, "Diffraction-pattern sampling for automatic pattern recognition," *Proc. IEEE* **58**, 198–216 (1970).
- D. E. Krueger, E. Rogot, W. C. Blackwelder, and D. D. Reid, "The predictive value of a postal questionnaire on cardio-respiratory symptoms," *J. Chronic Diseases* **23**, 411–421 (1970).
- N. George, J. T. Thomasson, and A. Spendel, "Photodetector light pattern detector," U.S. patent 3,689,772, (5 September 1972).
- J. K. Brouil and D. R. Smith, "A threshold logic network for shape invariance," *IEEE Trans. Electron. Comput.* **EC-16**, 818–828 (1967).
- C. F. Weiman and G. Chaikin, "Logarithmic spiral grids for image processing and display," *Computer Graphics and Image Processing* **11**, 197–226 (1979).
- E. L. Schwartz, "Afferent geometry in the primate visual cortex and the generation of neuronal trigger features," *Biol. Cybernetics* **28**, 1–14 (1977).
- G. M. Robbins and T. S. Huang, "Inverse filtering for linear shift-variant imaging systems," *Proc. IEEE* **60**, 862–872 (1972).
- D. Casasent and D. Psaltis, "Position, rotation, and scale invariant optical correlation," *Appl. Opt.* **15**, 1795–1799 (1976).
- L. Cohen, "The scale representation," *IEEE Trans. Signal Process.* **41**, 3275–3292 (1993).
- J. L. Pech-Pacheco, J. Alvarez-Borrego, and G. C. Matthias-Keil, "Automatic object identification irrespective to geometric changes," *Opt. Eng.* **42**, 551–559 (2003).

29. P. E. Zwicke and I. Kiss, "A new implementation of the Mellin transform and its application to radar classification of ships," *IEEE Trans. Pattern Anal. Mach. Intell.* **PAMI-5**, 191–199 (1983).
30. E. J. Zalubas and W. J. Williams, "Discrete scale transform for signal analysis," in *International Conference Acoustics on Speech, and Signal Processing IEEE*, 1995, Vol. 3, pp. 1557–1560.
31. D. Djurdjanovic, W. J. Williams, and C. K. Koh, "Discrete implementations of scale transform," *Proc. SPIE* **3807**, 522–533 (1999).
32. A. De Sena and D. Rocchesso, "A fast Mellin and scale transform," *EURASIP J. Appl. Signal Process.* **2007**, 089170 (2007).
33. J. R. Lerma-Aragón and J. Álvarez-Borrego, "Vectorial signatures for invariant recognition of position, rotation and scale pattern recognition," *J. Modern Opt.* **56**, 1598–1606 (2009).
34. A. Coronel-Beltrán and J. Álvarez-Borrego, "Comparative analysis between different font types and styles letters using a nonlinear invariant digital correlation," *J. Mod. Opt.* **57**, 58–64 (2010).
35. A. Solís-Ventura, J. Álvarez-Borrego, and S. Solorza, "Adaptive nonlinear correlation with a binary mask invariant to rotation and scale," *Opt. Commun.* **339**, 185–193 (2014).
36. S. M. Mehjabin, T. Shih, T. Renu, and M. S. Shahriar, "Incorporation of polar Mellin transform in a hybrid optoelectronic correlator for scale and rotation invariant target recognition," *J. Opt. Soc. Am. A* **31**, 1259–1272 (2014).
37. J. Gamboa, M. Fouda, and S. M. Shahriar, "Demonstration of shift, scale, and rotation invariant target recognition using the hybrid opto-electronic correlator," *Opt. Express* **27**, 16507–16520 (2019).
38. C. Barajas-García, S. Solorza-Calderón, and J. Álvarez-Borrego, "Classification of fragments of objects by the Fourier masks pattern recognition system," *Opt. Commun.* **367**, 335–345 (2016).
39. E. Garza-Flores and J. Álvarez-Borrego, "Pattern recognition using binary masks based on the fractional Fourier transform," *J. Modern Opt.* **65**, 1634–1657 (2018).
40. A. Castro-Valdez and J. Álvarez-Borrego, "Identification of phytoplankton species using Hermite transform," *Ukr. J. Phys. Opt.* **19**, 106–120 (2018).
41. A. Solís-Ventura, "Metodología basada en la transformada de escala y técnicas de correlación no lineal con invariancia a distorsiones geométricas e iluminación," Ph.D. thesis (CICESE, 2015).
42. A. Sánchez-Bruno and A. B. del Rosal, "Transformación Z de Fisher para la determinación de intervalos de confianza del coeficiente de correlación de Pearson," *Psicothema* **17**, 148–153 (2005).